UNCERTAINTIES IN TIR HYPERSPECTRAL IMAGE CUBE UNMIXING

Keshav Dev Singh and Ramakrishnan Desikan

Department of Earth Sciences, Indian Institute of Technology Bombay, Powai, Mumbai-400076, India

ABSTRACT

The spectral unmixing in the thermal infrared (TIR) region is not linear case. For simplicity, the spectral mixing for pixel deconvolution is assumed to be linear, but in reality, the intimate mixture spectra are non-linear. The multiple scattering effects due to texture and fabric do affect the spectral shape and form. In this paper, the uncertainties in unmixing of TIR hyperspectral image cube are investigated.

Index Terms— Thermal infrared, Hypercube, Non-linearity, Spectral unmixing

1. INTRODUCTION

Hyperspectral remote sensing in the thermal infrared (214m) region is a very recent development. Rocks and minerals typically provide diagnostic spectral features only in the thermal region. The spectral range of 2.5 to 13.5m is specifically dominated by emitted radiations and perfectly suited for spectral features detection [1]. This study addresses the problem to understand the association of spectral non-linearity in the thermal infrared (TIR) region. Using model-based unmixing, a non-linear mixing model (NLMM) can be formulated using a function f as in eqn. (1),

$$r_i = f(m_l, \xi_l, \rho, \eta; \lambda) \tag{1}$$

where, $r \in \Re^{n\times 1}$ and $m_l \in L_{n\times l}(library); l = 1, ..., q$. The abundance vector $\xi_l = \xi_1, \xi_2, ..., {\xi_q}^T$. Such unknown non-linear function depends upon the spatial extent, material fractions, media parameters (ρ) and noise levels (η). The physical models do not easily lend themselves to simple mathematical solutions. The main difficulty is how to model these non-linearties when much of the necessary information is not available. Hence, tackling the spectral non-linearties and addressing it is the most difficult task. However, by using the Planck radiation law, the emissivity interaction of intimate mixtures in thermal infrared domain could be defined [2]. Most of the thermal hyperspectral remote sensing (THRS) researchers [3, 4] believed that spectral mixing phenomenon in emissive (TIR) domain is purely a linear process. Taking a clue from the parameters contributing to non-linearity, in this paper, the uncertainties in unmixing of TIR hyperspectral image cube are investigated.

The authors are thankful to Prof. Dr. Schlerfet at Gabriel Lippmann Institute, Luxembourg and Telops, Canada for acquiring hypercube. Authors acknowledge Department of Science and Technology, and Indian Institute of Technology Bombay, India for the project grant support.

2. METHODOLOGY

The Fig. 1 shows a schematic flow chart of the proposed methodology which will be further explored in the following sections to show the existence and cause of spectral non-linearity in emissive (TIR) domain.

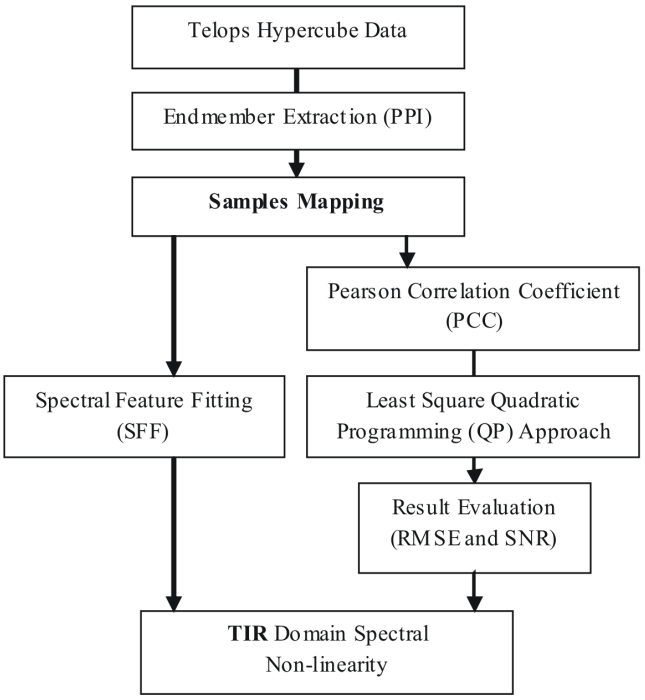


Fig. 1. Hierarchical diagram depicting the adopted methodology.

2.1. Thermal Hyperspectral Data Acquisition

In this study, an imaging FTIR instrument (Telops Hyper-Cam-LW) available at Gabriel Lippmann Institute, Luxembourg is used to collect hyperspectral image in laboratory conditions which covers a spectral range of 8 to 12m. Three geological samples- alunite, limestone and quartz are used in this

research. For emissivity retrieval, the samples are arranged as shown in Fig. 2.

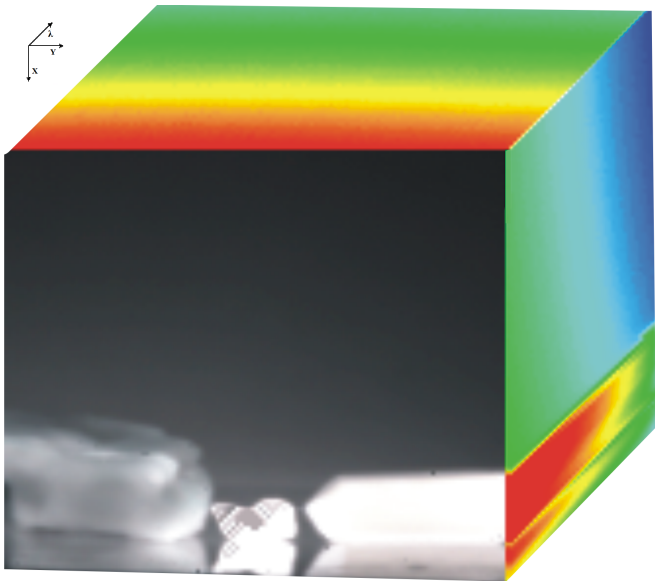


Fig. 2. Diagram showing surface of limestone, alunite and quartz sample respectively *(Image cube courtesy: Gabriel Lippmann Institute, Luxembourg)*.

The Telops Hyper-Cam measures a complete TIR hyperspectral image (128×128×81) with an instantaneous field-of-view of 0.35 mrad. It forms a hyperspectral image cube with n=81 spectral bands of number of pixels, p=16384 as shown in Fig. 3.



Fig. 3. Telops Hyper-Cam measured TIR hyperspectral image cube.

2.2. Endmember Extraction

Using ENVI, the noise in the data is reduced using Minimum Noise Fraction (MNF) technique and then Pixel Purity Index (PPI) are used for automatic endmember extraction. Spectrally pure pixels in the image are computed by projecting n-dimensional scatter plots onto the selected random vector for the threshold factor of 2.5 and iterations of 10,000. The nine endmembers showing characteristic absorption features (representing the chosen samples) are selected. Finally, these selected optimal set of endmembers are used for further analysis.

2.3. Spectral Unmixing

Once endmembers are derived, the Pearson Correlation Coefficient (PCC) is used to match these endmembers to each pixel of the image scene by Linear Mixing Model (LMM) developed in [5, 6]. Here, an iterative procedure based fully constrained quadratic programming algorithm is used to unmix each pixel of the hypercube [7]. It produces a vector of fractional abundances for individual endmembers on pixel-by-pixel basis and generates nine classified images representing each endmember.

2.4. Accuracy Assessment

The Root-Mean-Square Error (RMSE) and generalized Signal-to-Noise Ratio (SNR) is used to measure the uncertainties between the original (r_i) and modeled (M_i) image pixel spectra. The RMSE and SNR is defined as in eqn. (2),

$$\text{RMSE} = \sqrt{\frac{1}{n}\sum_{i=1}^{n}\eta(\lambda)_i^2}; where, \eta = \parallel r_i - M_i \parallel$$

$$SNR = 10 \times log_{10}\left(\frac{\sum_{i=1}^{n}\|r_i - M_i\|^2}{\sum_{i=1}^{n}\|r\|^2}\right) dB \qquad (2)$$

Where, n is the total number of wavelength (λ) channels.

3. RESULTS AND DISCUSSIONS

By using the SFF technique, the image is mapped for limestone, alunite and quartz respectively as shown in Fig. 4. In Fig. 4 (a) and (b) we can clearly see that limestone and alunite boundary is completely mapped. On the contrary, some portions ($\sim$ 2-3 inches) at the extreme left of quartz crystal (black color pixels) remain unmapped (Fig. 4 (c)). Also in Fig. 4 (b), the extreme left of the quartz crystal (white color pixels) are mapped as a mixture of alunite and quartz. Certain facets of quartz crystal showing the signature of alunite is not expected, if the process had been linear and single scattering. Further, unmapped regions of quartz, limestone and alunite may be caused by interaction of emitted energy coming from objects of different thermal properties and temperatures. Variation in thermal conductivity will determine the rate of the dissipation of heat, and hence, the brightness temperature of the target over time. For example, the thermal conductivity at room temperature (20 °C) of quartz mineral (20 W/m °C) is relatively higher than alunite (5 W/m °C) and limestone (6 W/m °C). Under such circumstances, objects heated

to specific constant temperatures will reach thermal equilibrium with the ambience at different rates. This temperature gradient will result in differential radiance from the objects and hence, non-linear mixing/bouncing of photons. Hence, there could be coupling of emitted radiation from different surface components of alunite, limestone and quartz crystal, which could result in such spectral non-linearity and uncertainty zone.

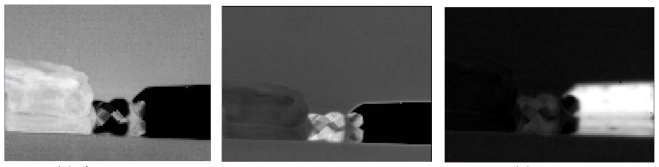


Fig. 4. Hypercube mapping with (a.) Limestone, (b.) Alunite, and (c.) Quartz using SFF.

The thermal-infrared (TIR) radiance directly consists of reflected and emitted radiance from the adjacent scene samples. The apparent emissivity is reduced by reflected radiation because the emissivity (ε) and reflectivity (ρ) are always complementary to each other (Kirchhoff's law). If materials are close enough, then radiation emitted by each material is absorbed by the adjacent materials. They may then be emitted later by the other materials. This process of absorption and emission give rise to higher non-linearity. In some cases, emitted radiation from one sample has been transmitted through the other adjacent sample and then emitted towards the sensor. Thus, the presence of alunite spectral feature on certain faces of quartz sample conveys that the emission spectroscopy is clearly not a case of linear spectral mixing. In Fig. 5 the elliptical portion shows precisely the higher uncertainty area due to the dominance of alunite emissivity over quartz.

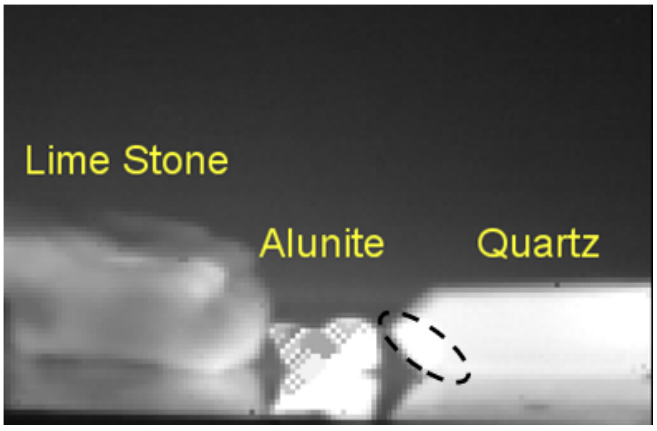


Fig. 5. TIR hyperspectral data showing unmapped area (dotted ellipse) at extreme left of quartz crystal.

The derived emissivity spectra for limestone, alunite, quartz, and mixed alunite-quartz zone (most uncertain elliptical region) are shown in Fig. 6.

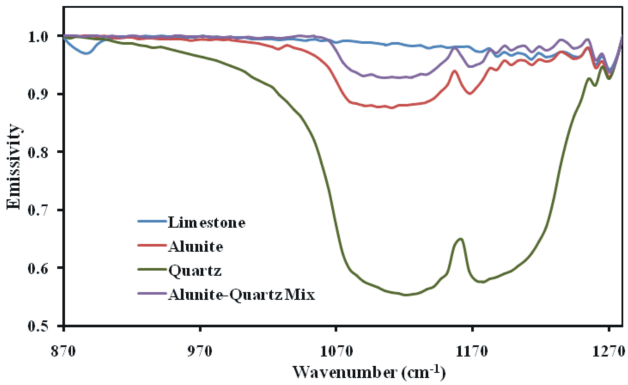


Fig. 6. Derived emissivity profiles for limestone, alunite, quartz, and mixed alunite-quartz.

Fig. 7 shows a fractional abundance image for each endmember, obtained from the linear spectral unmixing (DWT+PCC+FCQPA). In these abundance maps, the dark black pixels represent the lowest fractions value (0), different shades of grey color indicate increasing abundance, and exact white pixels indicate the maximum fractions value (1). Thus, the endmembers 1 to 4 are identified to represent quartz, 5 and 6 as limestone, 8 and 9 as alunite. The endmember 7 clearly indicates that it is a mixture of alunite and quartz. Pixels representing value 1 in the classified map typically indicate purest pixels. Whereas, pixels with values lower than 1 indicate mixed nature of spectra. The pixels that could not be resolved with the chosen set of endmembers (0 values) usually appear dark.

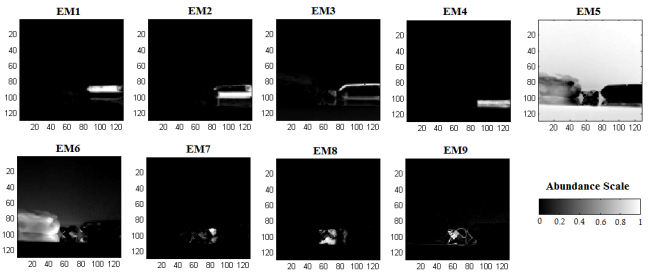


Fig. 7. Fractional abundance maps estimated from nine endmembers (EM) using FCLSE (QP) algorithm.

To understand the variations in spectral similarity between pure pixels and mix pixels, a RMSE image (Fig. 8) is obtained after taking root mean square difference between actual and estimated modeled spectra for each image pixel. The elliptical area in Fig. 8 can be qualitatively compared with Fig. 5 for maximum RMSE zones (yellow color dotted ellipse). This

can be addressed more clearly by plotting image pixel's Signal to Noise Ratio (SNR) peaks in a 3D shaded surface (Fig. 9). The encircled portion in Fig. 9 indicates minimum SNR peaks corresponding to maximum uncertainty.

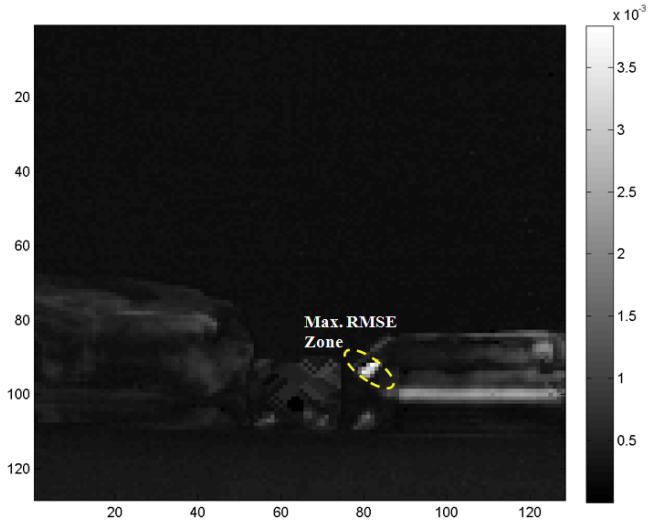


Fig. 8. RMSE image generated using the pure signatures of quartz, alunite, and limestone.

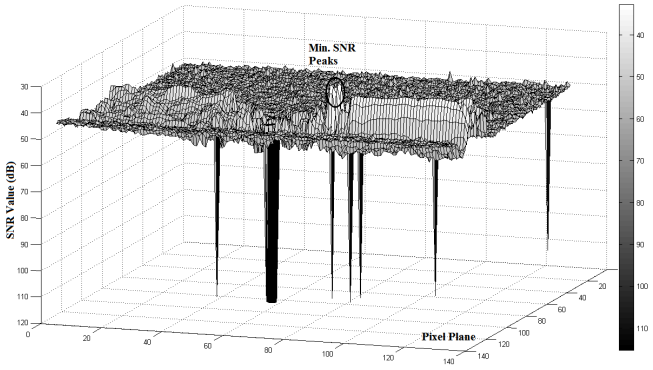


Fig. 9. 3D view of signal-to-noise ratio of each image pixel.

Thus, the analysis of SFF mapped images, RMSE and SNR image clearly indicates the regions of spectral mixing. These pixels show abnormal deviations from the reality and certainly are the result of mixing/contamination of radiation from adjacent objects. This is mainly attributed to multiple scattering from objects. The magnitude of such multiple scattering depends on the relative fractional covers of the samples and the wavelength.

4. CONCLUSIONS

It can be concluded, that even in thermal infrared (TIR) region, the photons undergo multiple scattering and result in non-linear mixing. It is generally caused by coupling of emitted radiance between spatially adjacent objects with heterogeneous thermal properties. In particular, spatial variations on thermal properties could be used during intimate mixtures mapping to formulate the non-linear function. The analytical procedures presented in this work can be used as a guideline for evaluating the mapping accuracy of hyperspectral images in the TIR region.

5. REFERENCES

[1] M. Schlerf, G. Rock, P. Lagueux, F. Ronellenfitsch, M. Gerhards, L. Hoffmann, and T. Udelhoven, "A Hyperspectral Thermal Infrared Imaging Instrument for Natural Resources Applications," *MDPI-Remote Sensing*, vol. 4, pp. 3995–4009, 2012.

[2] G. Fontanilles and X. Briottet, "A nonlinear unmixing method in the infrared domain," *Applied Optics*, vol. 50, pp. 3666–3677, 2011.

[3] M. S. Ramsey and P. R. Christensen, "Mineral abundance determination: Quantitative deconvolution of thermal emission spectra," *Journal of Geophysical Research*, vol. 103, pp. 577–596, 1998.

[4] S. A. Nowicki and P. R. Christensen, "Rock abundance on Mars from the Thermal Emission Spectrometer," *Journal of Geophysical Research*, vol. 112, no. E05007, pp. 1–20, 2007.

[5] K. D. Singh, D. Ramakrishnan, and L. Mansinha, "Relevance of transformation techniques in rapid endmember identification and spectral unmixing: A hypespectral remote sensing perspective," in *IEEE Geoscience and Remote Sensing Symposium (IGARSS), Munich, Germany*, July 2012, pp. 4066–4069.

[6] K. D. Singh, D. Ramakrishnan, and L. Mansinha, "A novel method for automatic minerals identification and their abundance estimation for material type discrimination using hyperspectral data," in *IEEE Workshop on Hyperspectral Image and Signal Processing: Evolution in Remote Sensing (WHISPERS), Shanghai, China*, June 2012, pp. 1–4.

[7] D. Heinz and C.-I. Chang, "Fully constrained least squares linear spectral mixture analysis method for material quantification in hyperspectral imagery," *IEEE Trans. Geosci. Remote Sensing*, vol. 39, no. 3, pp. 529545, 2001.